UNIVERSITAT DE BARCELONA

Facultat de Física
Barcelona, Spring 2020

Event horizon in a compact binary coalescence

Daniel Marín Pina
Advisor: Roberto Emparan

Master in Astrophysics, Particle Physics and Cosmology
Specialisation in Particle Physics and Gravitation

MASTER THESIS

To my family, friends and Laia
Special thanks to Dr. Emparan for his guidance and help
and to Dr. Martínez for her early collaboration in the project

Abstract

In this work we introduce a general method, mostly analytical with relatively simple numerics, for obtaining the event horizon in a compact binary coalescence in which one of the components is a supermassive black hole with a mass much greater than its companion's. We not only reproduce previous literature but also go beyond it by not restricting the smaller object to be a black hole. We apply this procedure to study the mergers of the large black hole with: (a) a Schwarzschild black hole, (b) a charged black hole, (c) a charged singularity and (d) several models of neutron stars. For the uncharged black hole, we recover the exact results in the literature using a slightly different method for solving (numerically) the equations. For the charged case, our results agree qualitatively with the results for the event horizon in the neutral case. For the charged singularity, we find that a "hole" (not a black hole) appears in the event horizon, due to the repulsive gravitational effect of the singularity, which we argue is physically pathological. For neutron stars, we discover that the structure of the merger depends on their compactness: above a certain threshold, the supermassive black hole induces the formation of a black hole inside the star, thus making the merger to happen "inside-out" in a phenomenon that we have named "precursory collapse". Our study of the mergers between neutron stars and black holes has given rise to an article that we have submitted for publication.

Contents

1 Introduction

Compact binary coalescences are among the most violent and extreme processes in nature, where the collision and fusion of two of the densest objects in the Universe releases energies of the order of multiple solar masses [2]. Far from a theoretical speculation, these events are routinely observed in gravitational-wave observatories (for a list of detections up to August 25, 2017, see [3]; newest events are reported in [10]). Although the experimental accessibility to gravitational radiation focuses most theoretical research towards it, in this report we will study the causal structure of the mergers and, in particular, the event horizon.

A black hole is defined as the spacetime region that is not in the causal past of future null infinity $\mathcal{I}^+$. The boundary of this region, and therefore of the black hole itself, is called the event horizon. This causal definition formalises the notion of the black hole as a region from which nothing can ever escape. In general, if we wanted to obtain the event horizon of a highly dynamical process such as a compact binary coalescence, we would need to perform numerical simulations of General Relativity in which spacetime is approximated by a discrete grid. In order to do so, we would need supercomputer-class hardware. This complexity makes the task daunting at first look, but it was realised [8] that there existed a subset of mergers for which this could be done easily, even in analytical form. This subclass are extreme-mass-ratio (EMR) coalescences, in which one component is a black hole and has a mass much larger than the other. Apart from the theoretical importance of EMR coalescences, it is a very active field in experimental astronomy, as the first detection of a binary coalescence with asymmetric masses [11] was reported during the writing of this Master's thesis.

Our aim with this work is twofold: first, we present a general method to obtain the event horizon in compact binary coalescences with extreme mass ratios. Secondly, we use the generality of the method to not only characterise mergers between two black holes, but between a charged and uncharged black hole and between a black hole and a neutron star.

2 Methodology

2.1 Extreme mass ratio argument

The key argument of this work is the application of the equivalence principle to guarantee that the spacetime curvature near a black hole vanishes at scales much smaller than its mass. This implies that the metric induced in the spacetime by an object of mass M near a black hole M_{SMBH} can be approximated by the metric of the object alone if $M \ll M_{\mathrm{SMBH}}$. As anticipated, this approximation, called "extreme mass ratio", is useful for studying binary coalescences in which one of the components is a supermassive black hole, although at the expense of losing the tidal forces associated to the curvature gradient.

The event horizon of a black hole is defined by a congruence of null geodesics. In this approximation, at very late times (specifically, at future null infinity $\mathcal{I}^+$) the congruence becomes planar. This specifies the asymptotic conditions for null rays, from where the merger can be resolved by tracing them back in time using the equations of motion of the metric induced by the infalling object alone.

Although this framework has already been applied in the literature (see [8, 9]), our proposal is novel in the fact that we will not restrict ourselves to astrophysical binary black holes. In particular, we will characterise mergers that include charged black holes and different models of neutron stars.

In a practical manner, our procedure will be as follows: we begin by finding the metric induced by the objects of our interest. The equivalence principle lets us fix the centre-of-mass reference frame, so we can use the conventional forms of the metrics as given in the literature. Then, we derive the relevant equations of motion for the null rays, for which we fix the boundary conditions at $\mathcal{I}^+$ to match a null plane. Finally, we numerically integrate these equations backwards in time up to the point where they focus and cross each other (the caustic line).

2.2 Derivation of the equations for the null geodesics

As argued above, we must begin by introducing the metric induced in the spacetime by the infalling object alone, in its rest frame. A general metric has many independent components which may depend on the coordinates, but it is possible to take very broad assumptions to greatly reduce its degrees of freedom for the problem at hand. In particular, we are considering very compact objects, potentially astrophysical in origin. Two hypotheses arise naturally: first, the object is compact enough to have collapsed under its own gravity; secondly, it is at equilibrium. These hypothesis can be translated to the metric, so we now require a static, spherically symmetric metric. It can be proven [15] that such metric can be expressed in the form

$$\mathrm{d}s^2 = -g_{tt}\mathrm{d}t^2 + g_{rr}\mathrm{d}r^2 + r^2\mathrm{d}\Omega^2 \tag{2.1}$$

where the only non-trivial components g_{tt} and g_{rr} are functions of r alone.

Although the naïve approach to obtain the null geodesics would be to use Killing vectors, we will be working in the Hamiltonian formulation. This formalism has the

advantage that the resulting equations will be much easier to solve numerically, specifically it avoids the problems in the change of the signs of square roots (see [9]). The hamiltonian for the null rays is

$$H = \frac{1}{2} g^{\mu\nu} p_\mu p_\nu = \frac{1}{2}\left(\frac{p_t^2}{g_{tt}} + \frac{p_r^2}{g_{rr}} + \frac{p_\theta^2}{r^2} + \frac{p_\phi^2}{r^2 \sin^2\theta}\right) \tag{2.2}$$

the equations of motion are derived using

$$\frac{\mathrm{d}x^\mu}{\mathrm{d}\lambda} = \frac{\partial H}{\partial p_\mu} \qquad ; \qquad \frac{\mathrm{d}p_\mu}{\mathrm{d}\lambda} = -\frac{\partial H}{\partial x^\mu} \tag{2.3}$$

Since H does not depend explicitly on t or ϕ, the associated momenta are conserved. Indeed, they are associated with the energy and angular momentum

$$p_t = -E \qquad ; \qquad p_\phi = L \tag{2.4}$$

Given that we are considering null rays, we will work with the parametrisation that makes $E = 1$. Furthermore, if our initial conditions are such that $L = 0$, then p_θ is conserved. We will define this quantity as q. We are left with

$$H = \frac{1}{2}\left(\frac{p_t^2}{g_{tt}} + \frac{p_r^2}{g_{rr}} + \frac{p_\theta^2}{r^2}\right) \tag{2.5}$$

So the only relevant equations of motion are

$$\frac{\mathrm{d}t}{\mathrm{d}\lambda} = -\frac{1}{g_{tt}} \tag{2.6}$$

$$\frac{\mathrm{d}r}{\mathrm{d}\lambda} = \frac{p_r}{g_{rr}} \tag{2.7}$$

$$\frac{\mathrm{d}\theta}{\mathrm{d}\lambda} = \frac{q}{r^2} \tag{2.8}$$

$$\frac{\mathrm{d}p_r}{\mathrm{d}\lambda} = \frac{1}{2g_{tt}^2}\frac{\mathrm{d}g_{tt}}{\mathrm{d}r} + \frac{p_r^2}{2g_{rr}^2}\frac{\mathrm{d}g_{rr}}{\mathrm{d}r} + \frac{q^2}{r^3} \tag{2.9}$$

2.3 Asymptotic conditions for the geodesics

The above differential equations determine the geodesics up to four integration constants. These constants are computed by matching the geodesics with a null plane at $\mathcal{I}^+$, meaning that the end result of the merger is a black hole at equilibrium. Due to the assumptions taken in the previous section about the infalling object (that it is static and spherical), the Maxwell-Birkhoff theorem guarantees that at very large distances from it the metric of the spacetime will match exactly the Reissner-Nordström solution. Therefore, we will be able to compute the asymptotic conditions for the geodesics in general instead of a case-by-case basis. The approach that we will follow is the same than in the literature (see [9], although in our case we do not consider rotation but charge). We begin by taking the Reissner-Nordström metric

$$\mathrm{d}s^2 = -\left(1 - \frac{2M}{r} + \frac{Q^2}{r^2}\right)\mathrm{d}t^2 + \frac{\mathrm{d}r^2}{1 - \frac{2M}{r} + \frac{Q^2}{r^2}} + r^2 \mathrm{d}\Omega^2 \tag{2.10}$$

The form of (2.6)-(2.8) for this metric is

$$\frac{\mathrm{d}t}{\mathrm{d}\lambda} = \frac{1}{1-\frac{2M}{r}+\frac{Q^2}{r^2}} \tag{2.11}$$

$$\frac{\mathrm{d}r}{\mathrm{d}\lambda} = \left(1-\frac{2M}{r}+\frac{Q^2}{r^2}\right)p_r \tag{2.12}$$

$$\frac{\mathrm{d}\theta}{\mathrm{d}\lambda} = \frac{q}{r^2} \tag{2.13}$$

$$\frac{\mathrm{d}p_r}{\mathrm{d}\lambda} = \frac{r^4(Q^2-Mr)+q^2(Q^2+r(r-2M))^2+pr^2(Q^2-Mr)(Q^2+r(r-2M))^2}{r^3(Q^2+r(r-2M))^2} \tag{2.14}$$

From $p^\mu p_\mu = 0$ we obtain an explicit equation for $p_r(r)$

$$p_r = \frac{\sqrt{1-\left(1-\frac{2M}{r}+\frac{Q^2}{r^2}\right)\frac{q^2}{r^2}}}{1-\frac{2M}{r}+\frac{Q^2}{r^2}} \tag{2.15}$$

which can be used to decouple the equation for $\frac{\mathrm{d}r}{\mathrm{d}\lambda}$. Nevertheless, it will be preferable to substitute and integrate the inverse equation $\frac{\mathrm{d}\lambda}{\mathrm{d}r}$ and then invert the solution. Since the late-time asymptotics correspond to large values of the radial coordinate, we can work with an expansion over $1/r$

$$\frac{\mathrm{d}\lambda}{\mathrm{d}r} = \frac{1}{\sqrt{1-\left(1-\frac{2M}{r}+\frac{Q^2}{r^2}\right)\frac{q^2}{r^2}}} = 1+\frac{q^2}{2r^2}-\frac{Mq^2}{r^3}+\mathcal{O}\left(r^{-4}\right) \tag{2.16}$$

$$r(\lambda) = r_\infty+\lambda+\frac{q^2}{2\lambda}-\frac{Mq^2}{2\lambda^2}+\frac{-\frac{q^4}{8}+\frac{q^2Q^2}{6}}{\lambda^3}+\mathcal{O}\left(\lambda^{-4}\right) \tag{2.17}$$

where we set the parameter r_∞ to zero using λ reparametrisation. This solution for r allows us to decouple the other equations

$$\frac{\mathrm{d}t}{\mathrm{d}\lambda} = 1+\frac{2M}{\lambda}+\frac{4M^2-Q^2}{\lambda^2}+\frac{8M^3-Mq^2-4MQ^2}{\lambda^3}+\mathcal{O}\left(\lambda^{-4}\right) \tag{2.18}$$

$$\frac{\mathrm{d}\theta}{\mathrm{d}\lambda} = \frac{q}{\lambda^2}+\mathcal{O}\left(\lambda^{-4}\right) \tag{2.19}$$

$$\begin{aligned} t(\lambda) = t_\infty+\lambda+2M\log\frac{\lambda}{2M}+\frac{-4M^2+Q^2}{\lambda}-\frac{M(8M^2-q^2-4Q^2)}{2\lambda^2} \\ +\frac{-16M^4-Q^2(q^2+Q^2)+3M^2(q^2+4Q^2)}{3\lambda^3}+\mathcal{O}\left(\lambda^{-4}\right) \end{aligned} \tag{2.20}$$

$$\theta(\lambda) = \theta_\infty-\frac{q}{\lambda}+\frac{q^3}{3\lambda^3}+\mathcal{O}\left(\lambda^{-4}\right) \tag{2.21}$$

Without loss of generality, we can set $t_\infty = 0$ and $\theta_\infty = 0$ by shifting the time origin and orientation of the null plane. The remaining asymptotic condition, that for the momentum, can be found directly with (2.15)

$$p_r(\lambda) = 1+\frac{2M}{\lambda}+\frac{4M^2-q^2/2-Q^2}{\lambda^2}+\frac{8M^3-Mq^2-4MQ^2}{\lambda^3}+\mathcal{O}\left(\lambda^{-4}\right) \tag{2.22}$$

2.4 Metric matching at the surface

Although the procedure outlined above is valid for any given metric with the stated properties, it can be generalised so we are able to use a metric defined by different functions in different regions of the spacetime. We will use this generalisation for the study of objects of finite radius R, such as neutron stars. In these kind of objects, the interior metric is found via equations of state, and is generally only valid for $r < R$. Furthermore, Birkhoff's theorem for the Einstein-Maxwell theory guarantees that the exterior metric is simply the Reissner-Nordström solution. The generalisation is easy in the fact that the only relevant change is that we must impose that the metric is continuous at $r = R$. Given two static, spherically symmetric metrics $\mathrm{d}s^2_{\text{int}}$ and $\mathrm{d}s^2_{\text{ext}}$

$$\mathrm{d}s^2_{\text{int}} = -g^{(\text{int})}_{tt}\mathrm{d}t^2_{(\text{int})} + g^{(\text{int})}_{rr}\mathrm{d}r^2_{(\text{int})} + r^2_{(\text{int})}\mathrm{d}\Omega^2 \tag{2.23}$$

$$\mathrm{d}s^2_{\text{ext}} = -g^{(\text{ext})}_{tt}\mathrm{d}t^2_{(\text{ext})} + g^{(\text{ext})}_{rr}\mathrm{d}r^2_{(\text{ext})} + r^2_{(\text{ext})}\mathrm{d}\Omega^2 \tag{2.24}$$

the metric they induce at the surface $r = R$ is

$$\mathrm{d}s^2_{\text{int}}(r = R) = -g^{(\text{int})}_{tt}(r = R)\mathrm{d}t^2_{(\text{int})} + R^2\mathrm{d}\Omega^2_{\text{int}} \tag{2.25}$$

$$\mathrm{d}s^2_{\text{ext}}(r = R) = -g^{(\text{ext})}_{tt}(r = R)\mathrm{d}t^2_{(\text{ext})} + R^2\mathrm{d}\Omega^2_{\text{ext}} \tag{2.26}$$

For the two induced metrics to be the same, we can let the coordinates r, θ and ϕ to be identical inside and outside $r = R$. Therefore, we only have to match the t coordinate. Let us define

$$\chi \equiv \frac{\mathrm{d}t_{(\text{int})}}{\mathrm{d}t_{(\text{ext})}} = \sqrt{\frac{g^{(\text{ext})}_{tt}(r = R)}{g^{(\text{int})}_{tt}(r = R)}} \tag{2.27}$$

Now, if we want to match our previous procedure, we have to identify $t = t_{(\text{ext})}$. The generalisation becomes very simple: when dealing with equations of motion at $r < R$, we have to make the substitution

$$\mathrm{d}t \;\mapsto\; \frac{\mathrm{d}t}{\chi} \tag{2.28}$$

Note that this procedure is consistent since $\chi = 1$ when the metric is described by a single function.

2.5 Relative motion

In the above sections we have developed the method for a radial infall, even though the mergers found in nature generically happen at skewed collision angles. Furthermore, we have not taken into account the spin of the larger black hole, which need not be negligible. This shall not be a problem, as we will now argue that the structure of the mergers is independent of these quantities and the results for the radial, non-rotating case are always valid.

In the extreme-mass-ratio limit, the spin of the larger black hole is indistinguishable from a skewed collision angle, so all the possible relative motion can be described as the

combination of parallel and perpendicular movement with respect to the event horizon of the supermassive black hole. The former is trivially irrelevant in this limit, since the asymptotic surface from which the horizon is traced back is invariant under boosts. For the movement parallel to the supermassive black hole, it can be proven [8] that a relative rapidity η can be integrated to our asymptotic conditions simply by setting the parameter θ_∞ as

$$\sin\theta_\infty = \tanh\eta \tag{2.29}$$

As we have argued above, the choice of θ_∞ only affects the orientation of the merger, so fixing $\theta_\infty = 0$, $\eta = 0$ does not imply loss of generality.

3 Charged black holes

3.1 General properties

The first compact object that we will consider are charged black holes. These objects are simple in the sense that they have a complete and exact description [14, 12] in classical general relativity, which, furthermore, depends on only two parameters: their mass M and charge Q. The exact form of this metric, called the Reissner-Nordström solution, is

$$\mathrm{d}s^2 = -\left(1 - \frac{2M}{r} + \frac{Q^2}{r^2}\right)\mathrm{d}t^2 + \frac{\mathrm{d}r^2}{1 - \frac{2M}{r} + \frac{Q^2}{r^2}} + r^2\mathrm{d}\Omega^2 \tag{3.1}$$

Depending on the values of the parameters, we can have notably different objects

Case $Q = 0$: Schwarzschild black hole
This is the simplest case: the black hole is uncharged and the solution reduces to the Schwarzschild solution. This analysis has already been carried out, even in an analytical form [8]. Far from discouraging, we will use this case to verify the validity of our computational modelling

Case $M > |Q|$: Reissner-Nordström black hole
In this case there is a black hole with two horizons $r_\pm$

$$r_\pm = M \pm \sqrt{M^2 - Q^2} \tag{3.2}$$

We will only be interested in the outer horizon r_+, which is an event horizon. The inner horizon r_- is a Cauchy surface.

Case $M < |Q|$: Charged singularity
This case represents a naked timelike singularity. Although all charged particles have $M < |Q|$, this solution predicts a region where gravity has a repulsive effect; below we will discuss and find that the gravitational field in this region is unphysical. Nevertheless, it will be interesting to study the mergers to probe the potential pathologies that would develop there.

Case $M = |Q|$: Extremal Reissner-Nordström black hole
This case represents the limit of $M > |Q|$ when $M \to |Q|$. Now, $r = r_+$ is both an event horizon and a Cauchy surface. In general, one would expect this case to have some peculiarities over the $M > |Q|$ charged black hole. However, we will find that in the horizon of the merger, the limit $M \to |Q|$ makes no significant qualitative difference.

The equations of motion for the null geodesics are the same as those considered for the general asymptotic conditions (2.14), only that in this case they are valid for all values of the radial coordinate.

$$\frac{\mathrm{d}t}{\mathrm{d}\lambda} = \frac{1}{1 - \frac{2M}{r} + \frac{Q^2}{r^2}} \tag{3.3}$$

$$\frac{\mathrm{d}r}{\mathrm{d}\lambda} = \left(1 - \frac{2M}{r} + \frac{Q^2}{r^2}\right) p_r \tag{3.4}$$

$$\frac{\mathrm{d}\theta}{\mathrm{d}\lambda} = \frac{q}{r^2} \tag{3.5}$$

$$\frac{\mathrm{d}p_r}{\mathrm{d}\lambda} = \frac{r^4(Q^2 - Mr) + q^2(Q^2 + r(r-2M))^2 + pr^2(Q^2 - Mr)(Q^2 + r(r-2M))^2}{r^3(Q^2 + r(r-2M))^2} \tag{3.6}$$

Although in the previous section we have derived an explicit equation for p_r, we will now work with the coupled differential equation. As noted in [9], the change of sign of the root along the geodesics introduces a great deal of complexity that can be avoided.

3.2 Case $Q = 0$: Schwarzschild black hole

The numerical integration of the equations above yields only three independent functions: $t(\lambda)$, $t(\lambda)$ and $\theta(\lambda)$. Since the parameter λ is physically irrelevant, all the non-trivial information about the merger can be summarised in a single three-dimensional parametric plot. Instead of using t, r and θ as coordinates, we will use Cartesian-like coordinates with the usual definition of

$$x = r\sin\theta \tag{3.7}$$

$$z = r\cos\theta \tag{3.8}$$

$$t = t \tag{3.9}$$

The plot that we generate for the uncharged black hole can be found in figure 3.2. Although this plot displays all the obtainable physical information, its presentation may hinder our physical intuition. It is much simpler, then, to analyse its constant-time slices (see figure 3.1).

Although the analysis of these results has already been carried out in the literature (see [8]), it is worthwhile to reproduce it in here to define certain physical properties that will be useful for the posterior (novel) analyses of mergers. First, the (x, z, t) plot is a "pants diagram", where each "leg" (also called "throat") represents one of the original black holes. Since we are working in the extreme-mass-ratio limit, one of the legs is infinite in size and is therefore drawn as a flat surface. Secondly, for each black hole, the point on its event horizon closest to the other black hole forms a caustic line. We obtain this curve as a function of $q \neq 0$ by imposing that $\theta_{\text{caus}}(q) = -\pi$

$$\theta(\lambda \equiv \lambda_{\text{caus}}(q)) = -\pi \qquad \Longrightarrow \qquad \begin{cases} t(\lambda = \lambda_{\text{caus}}) = t_{\text{caus}}(q) \\ r(\lambda = \lambda_{\text{caus}}) = r_{\text{caus}}(q) \end{cases} \tag{3.10}$$

If we follow the caustics forward in time, we can see that they merge at the crotch area of the pants. The event corresponding to this merge, called the "pinch-on", is the point in spacetime where the event horizons of both black holes make contact. The coordinates of this event are $t = t_*$, $r = r_*$ and $\theta = -\pi$. Of the non-trivial components, t_* defines the boundary between two and one black holes and r_* is a measure of the maximum distortion of the small black hole. These components can be computed by searching for the local maximum of t_{caus} and are as follows

$$t_* = -7.53461M \tag{3.11}$$

$$r_* = 3.52061M \tag{3.12}$$

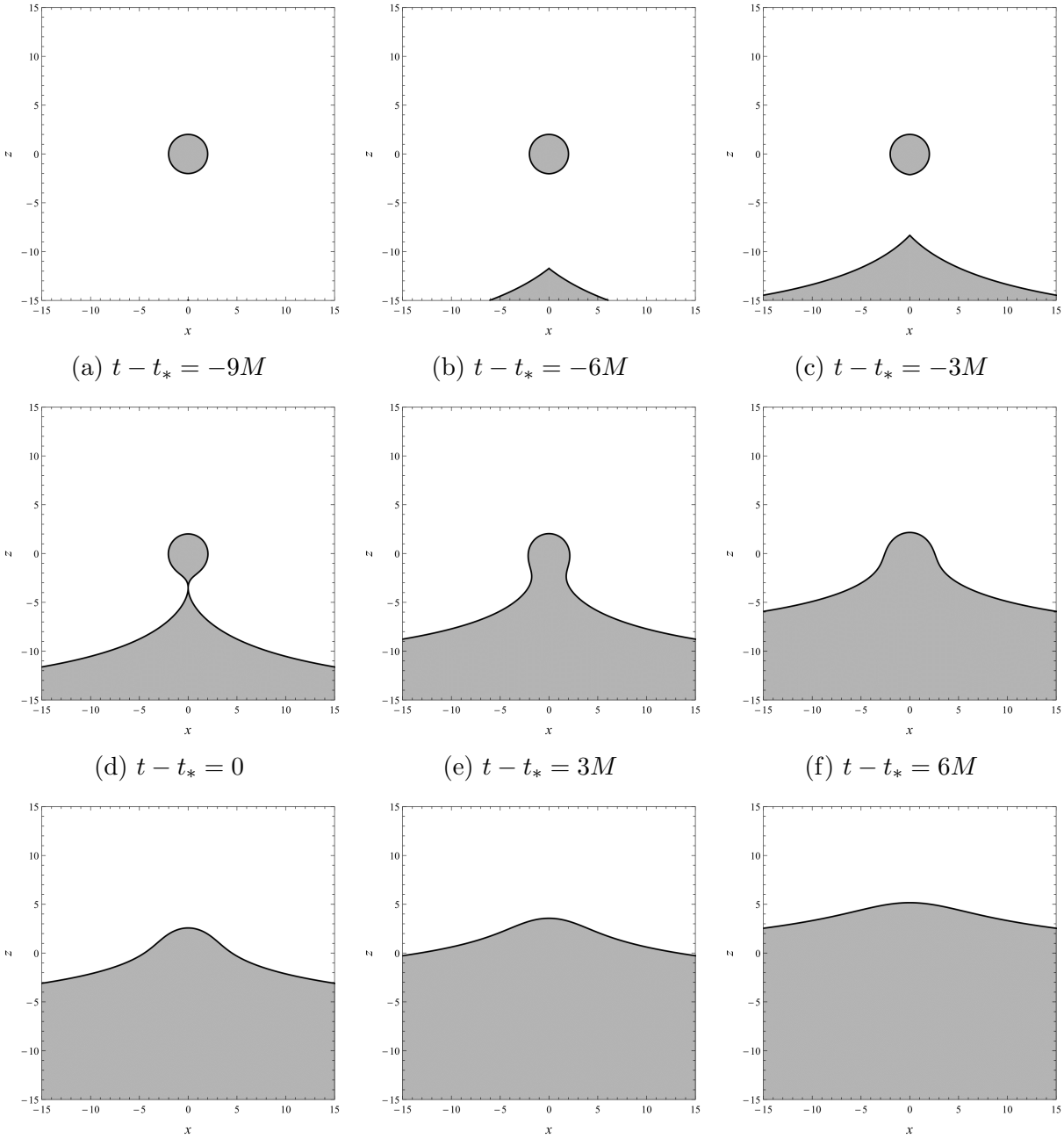

(a) $t - t_* = -9M$ (b) $t - t_* = -6M$ (c) $t - t_* = -3M$

(d) $t - t_* = 0$ (e) $t - t_* = 3M$ (f) $t - t_* = 6M$

(g) $t - t_* = 9M$ (h) $t - t_* = 12M$ (i) $t - t_* = 15M$

Figure 3.1: Constant-time slices of the event horizon in a merger of a supermassive black hole (down) with a Schwarzschild black hole (centre) in the latter's centre-of-mass reference frame. The event horizon is plotted with a black line, the grey area represents the inside of the black holes. The axes are measured in units of M. The time slices are taken at regular time intervals

which match the exact results in [8] up to the last significant digit, therefore proving that our uncertainties are of the order $\mathcal{O}\left(10^{-6}M\right)$. The exact value of t_* is determined up to a constant, corresponding to the arbitrary choice of t_∞. In this case, we have chosen the same time origin than in the reference, so the comparison is justified.

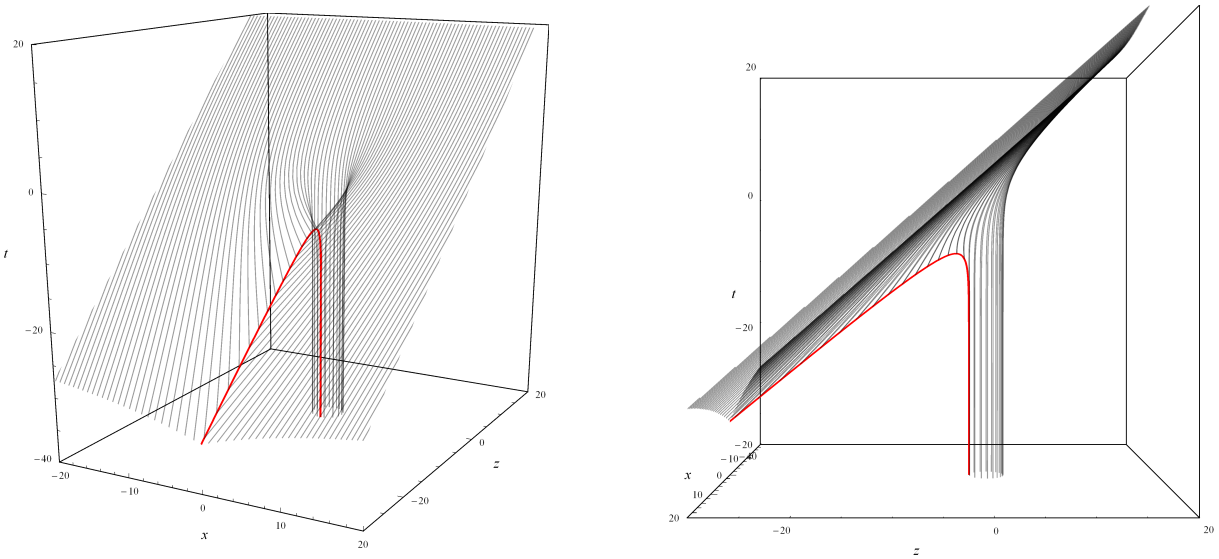

Figure 3.2: Event horizon in a merger of a supermassive black hole with a Schwarzschild black hole. The red curve represents the caustic line. The axes are measured in units of M.

3.3 Case $M > |Q|$: Charged black hole

The results that we obtain by solving (2.14) for $M > |Q|$ are represented in figure 3.3. As we can see, the general structure of the merger is the same as for the uncharged case. The only difference is that the throat of the diagram, which corresponds to the charged black hole at the $t \to -\infty$ limit of the merger, is smaller. This effect is quite easily interpreted, as now the event horizon of this black hole lies at $r_+ = M + \sqrt{M^2 - Q^2} < 2M$. This further justifies our assumption that the horizon at r_- does not play a role in these processes.

Although a charge $|Q| < M$ may not have an effect on the qualitative structure of the merger, it will be interesting to study the quantitative effects. In particular, we can obtain the coordinates of the pinch-on. Let us take the merger from figure 3.3, with $M = 1$ and $|Q| = 0.8$

$$t_* = -8.11498 \tag{3.13}$$

$$r_* = 3.06699 \tag{3.14}$$

Comparing with the respective results for $Q = 0$, $M = 1$ at (3.11) and (3.12), we can see that both these values are smaller in the charged case. In particular, the decrease in the radial component can easily be explained with the same argument as before: since the event horizon is at $r_+ < 2M$, the smaller black hole gets less distorted and the pinch-on happens closer to its centre.

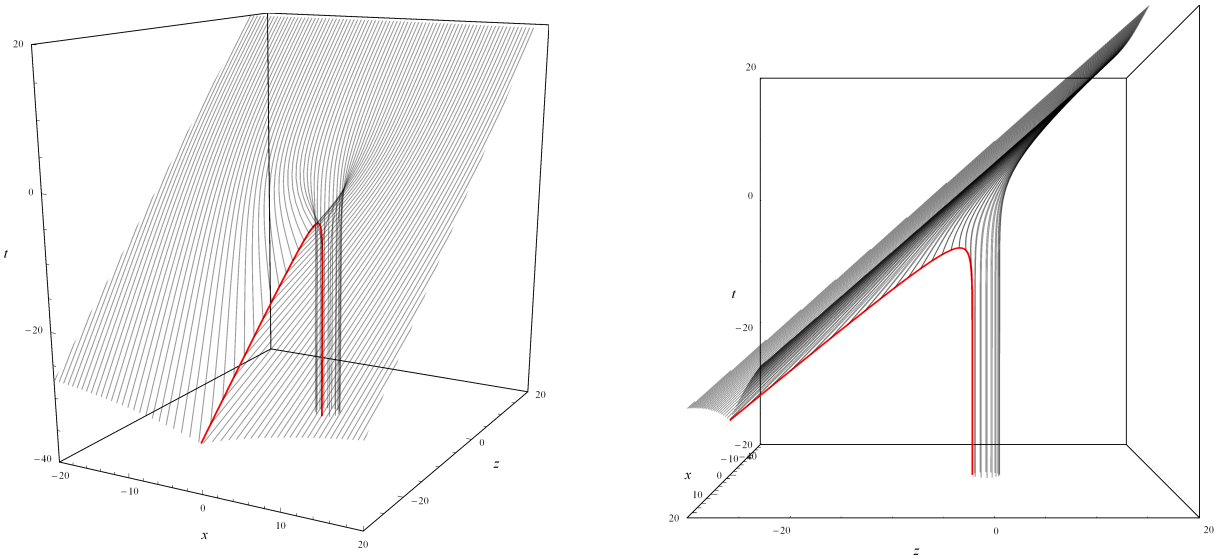

(a) (b)

Figure 3.3: Event horizon in a merger of a supermassive black hole with a charged black hole of $|Q| = 0.8$, $M = 1$. The red curve represents the caustic line. The axes are measured in units of M.

3.4 Case $M < |Q|$: Charged singularity

The next case that we will consider is $M < |Q|$. For these values of the parameters, the Reissner-Nordström metric describes a charged timelike singularity located at $r = 0$, so there is not an event horizon at a finite radius r. Although the equations to solve (2.14) are equal than in the previous case, we obtain mergers with a totally different structure.

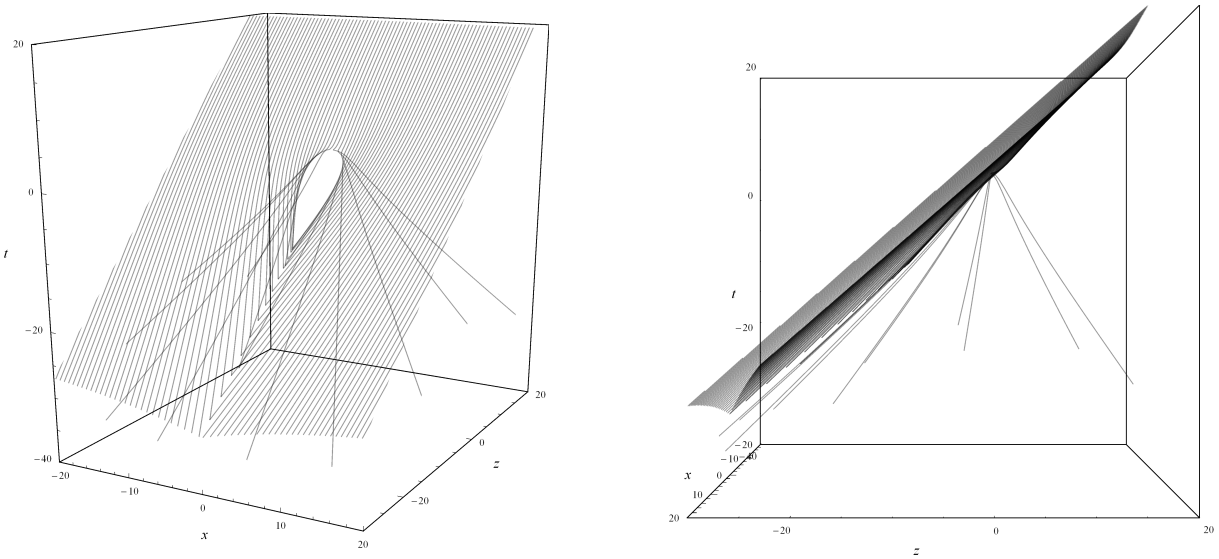

(a) (b)

Figure 3.4: Event horizon in a merger of a supermassive black hole with a charged singularity of $|Q| = 2$, $M = 1$. The red curve represents the caustic line. The axes are measured in units of M.

This merge has two key features: first, the pants diagram that we obtain does not have the thinner leg; this is due to the absence of a finite-radius black hole. Secondly, the event horizon of the larger black hole develops a "hole" when the singularity is close to it, with light rays emanating from its border. This is an unexpected behaviour which has never been reported in the literature, albeit we will show that it is not a new physical phenomenon but a consequence of failing to consider quantum-electrodynamical effects.

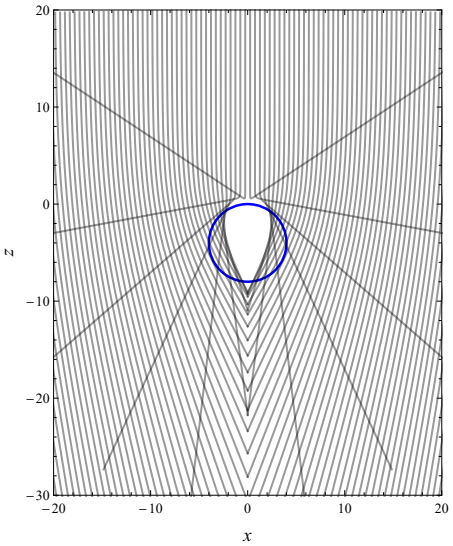

Figure 3.5: Structure of the merger projected in the (x, z) plane for a charged singularity with $M = 1$ and $Q = 2$. In gray, null geodesics of the event horizon. In blue, classical electron radius r_c

In order to argue for this point, let us consider the radial scale at which the QED effects become relevant and the classical Einstein-Maxwell theory breaks down. Namely, the Reissner-Nordström solution assumes that the electromagnetic field of the charge, and the stress-energy tensor of this field, are described by the classical Maxwell theory. However, this is not the case. At distances of the order of the Compton wavelength of the particle, $\sim 1/M$ (in natural units), virtual pair-production effects become important and modify the electric field around the particle, in such a way that the (renormalized) stress-energy tensor differs from the classical value, and in particular it diverges much less strongly at short distances. As a consequence, the Reissner-Nordström solution provides an appropriate description of the gravitational field that a charged (spinless) particle creates only down to distances $\sim 1/M$. We will not enter in the description of the corrected gravitational field, but we will describe now how the region in the $|Q| > M$ Reissner-Nordström metric where the gravitational field is repulsive is excised by this argument, and hence its pathological features are eliminated as unphysical. On simple grounds, we can say that if

$$g_{tt} + 1 = \frac{2M}{r} - \frac{Q^2}{r^2} \tag{3.15}$$

is negative, then the gravitational field has a repulsive effect (on charged or neutral particles). The radius at which this happens is

$$r_c = \frac{Q^2}{2M} \tag{3.16}$$

which is indeed the classical electron radius. In natural units we have $Q^2 \approx \alpha$ (the fine structure constant) so $Q^2 < 1$ and we see that r_c is smaller than the Compton radius $1/M$. All the gravitational repulsive effects are therefore eliminated. Observe that this resolution of the unphysical effects and divergences associated to the naked singularity of the solutions with $|Q| > M$ involves quantum electrodynamical effects but not quantum gravity: the gravitational field remains classical, and it is only the matter-radiation part of the system that is quantum.

Nevertheless, even if we have argued that the gravitational repulsive effects are not present in any known physical system, we find it interesting to see what would be their consequences on the event horizon of a merger.

3.5 Case $M = |Q|$: Extremal black hole

For completeness, it will be interesting to study the case of the extremal Reissner-Nordström black hole. Proceeding as the previous cases, we have generated figure 3.6. As we can see, the structure of the merger is the same as for the non-extremal charged black holes, which shows that the $M = |Q|$ case presents no qualitative peculiarities over $M > |Q|$. Furthermore, this result confirms that the Cauchy horizon does not play any role on our analysis, even when it matches r_+. The coordinates of the pinch-on are

$$t_* = -7.57100M \tag{3.17}$$

$$r_* = 2.72458M \tag{3.18}$$

In particular, this value for r_* constitutes a lower bound for mergers with a charged black hole.

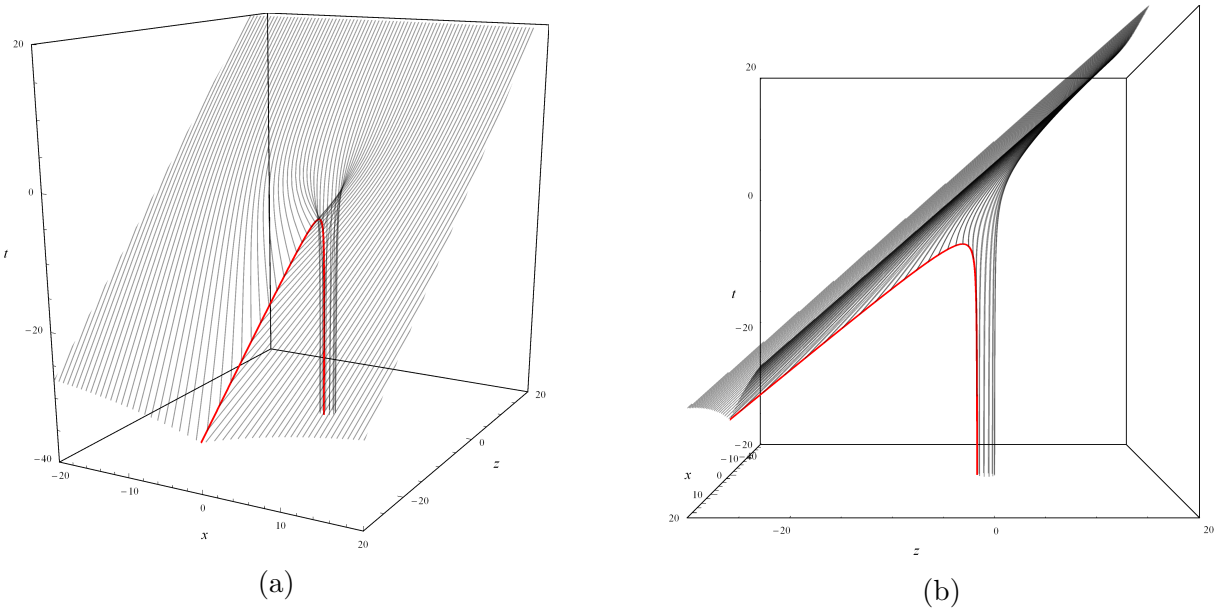

Figure 3.6: Event horizon in a merger of a supermassive black hole with an extremal charged black hole of $M = |Q| = 1$. The red curve represents the caustic line. The axes are measured in units of M.

4 Neutron stars

The second family of objects that we are going to study are neutron stars. Unlike for black holes, the metric that describes their interior is not known, so we will be forced to study the coalescences using different models. The models that we will consider are, from less to most realistic, the thin shell, constant density and Tolman VII solutions. These models are spherical, uncharged and static; therefore, we can apply the method presented in section 2 to determine their event horizon in an EMR compact binary coalescence. Far from being ad hoc hypotheses, these assumptions are well justified: the ellipticity of a neutron star is observationally bounded at $\epsilon \lesssim 7 \times 10^{-8}$ [1] and its charge is very roughly approximated by $100\frac{M}{M_\odot}$ C $\sim 6 \times 10^{-19}$ [4].

The models that we are going to study have some common properties. Their exterior $r > R$ is described by the Schwarzschild metric ($Q = 0$ limit of the Reissner-Nordström metric) and their interior depends only on the mass M and the radius R as r/R and M/R. This implies that the merger only has an independent variable, that we define to be the compactness β

$$\beta \equiv \frac{M}{R} \tag{4.1}$$

For simplicity, we will work with $M = 1$ and let $\beta = R^{-1}$.

4.1 Thin shell model

The first model that we are going to consider is the thin shell. This is the simplest model of an extended, massive object in general relativity: a homogeneous mass distribution located in a thin shell at $r = R$ with empty space inside and outside. Although this model does not reflect the internal structure of the neutron star, we will prove that it shares the general characteristics of the merger with other much more realistic models.

The interior metric for this object is simply the Minkowski metric; this is guaranteed by the Gauss theorem. The equations of motion in the interior are

$$\frac{\mathrm{d}t}{\mathrm{d}\lambda} = \frac{1}{\chi} \tag{4.2}$$

$$\frac{\mathrm{d}r}{\mathrm{d}\lambda} = p_r \tag{4.3}$$

$$\frac{\mathrm{d}\theta}{\mathrm{d}\lambda} = \frac{q}{r^2} \tag{4.4}$$

$$\frac{\mathrm{d}p_r}{\mathrm{d}\lambda} = \frac{q^2}{r^3} \tag{4.5}$$

and the metric continuity factor

$$\chi = \sqrt{1 - \frac{2M}{R}} \tag{4.6}$$

The solution to these equations yields figure 4.1. This model, although simple, showcases

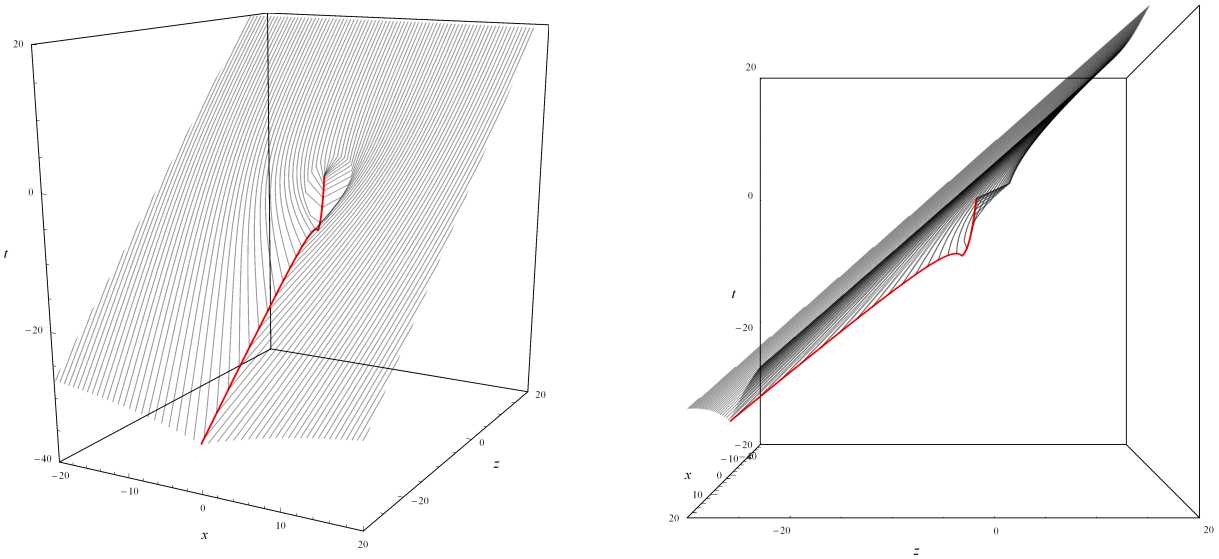

(a) (b)

Figure 4.1: Event horizon in a merger of a supermassive black hole with a thin shell of $R = 2.8$, $M = 1$ ($\beta = 0.36$). This merger presents a precursory collapse. The red curve represents the caustic line. The axes are measured in units of M.

many important features that we can use as a benchmark to characterise more physically acceptable models. In particular, we observe two regions: the exterior ($r > R$), which is equal to the Schwarzschild case, and the interior. The most notable feature of the latter is that it does not have a throat due to the neutron star not having an event horizon by itself. The angular points on the $r = R$ surface are only a manifestation of the thin shell effects and will disappear once we consider three-dimensional models.

The general structure of the merger at $r < R$ depends on β, with two separate behaviours. For small values of the compactness, the merger is as expected: the event horizon of the black hole engulfs the whole star, notably warping around the edges, where the matter is. For large values of the compactness, though, there is a surprising effect. A second event horizon develops in the stellar interior and merges with the large event horizon, so we could say that the neutron star coalesces with the black hole from the inside out. This effect can be seen in figure 4.1b as a spike corresponding to the local minimum of the caustic line. We have not found this double event horizon structure in the literature, therefore it is worth studying whether it appears in neutron star models with realistic equations of state. In the following sections we will show that this double horizon structure is real and physical, and furthermore that it can happen for acceptable values of the compactness. This discovery during the writing of this Master's thesis prompted the writing of a paper [7], were we have named the double horizon as "precursory collapse".

Note that, unlike the usual process of black hole formation due to the collapse of a star in the latter part of its life, this double structure is not associated to any collapse or movement of matter inside the star. In fact, the star does not suffer any kind of tidal deformation due to having taken the extreme-mass-ratio limit.

4.2 Schwarzschild interior solution

The next neutron star model that we are going to consider is the Schwarzschild interior solution, which describes a constant density sphere of mass M and radius R. Although this model is still unrealistic, it will constitute an improvement over the thin shell. In this regard, we expect the null rays to have a smooth behaviour when transiting the surface. For the double horizon effect, we will show that it still appears at sufficiently large values for the compactness, proving that it is not an artefact of the thin shell.

The Schwarzschild interior solution is

$$\mathrm{d}s^2 = -\frac{1}{4}\left(3\sqrt{1-\frac{2M}{R}} - \sqrt{1-\frac{2Mr^2}{R^3}}\right)^2 \mathrm{d}t^2 + \frac{\mathrm{d}r^2}{1-\frac{2Mr^2}{R^3}} + r^2\mathrm{d}\Omega^2 \tag{4.7}$$

so the equations of motion are

$$\frac{\mathrm{d}t}{\mathrm{d}\lambda} = \frac{4}{\left(3\sqrt{1-\frac{2M}{R}} - \sqrt{1-\frac{2Mr^2}{R^3}}\right)^2} \tag{4.8}$$

$$\frac{\mathrm{d}r}{\mathrm{d}\lambda} = \left(1-\frac{2Mr^2}{R^3}\right)p_r \tag{4.9}$$

$$\frac{\mathrm{d}\theta}{\mathrm{d}\lambda} = \frac{q}{r^2} \tag{4.10}$$

$$\frac{\mathrm{d}p_r}{\mathrm{d}\lambda} = \frac{q^2}{r^3} + \frac{2Mrp_r^2}{R^3} + \frac{8Mr}{\sqrt{1-\frac{2Mr^2}{R^3}}\left(\sqrt{1-\frac{2Mr^2}{R^3}}R - 3\sqrt{R\,(R-2M)}\right)^3} \tag{4.11}$$

Note that the coordinate choice of this solution yields $\chi = 1$

As expected, this solution presents many improvements over the thin shell. In this merger there are no angular points in the geodesics at $r = R$ and the interior is much more well-behaved (see figures 4.3, 4.4). As we can see in the plots, the double horizon ("precursory collapse") is still present in this model at sufficiently large values of the compactness. Namely, it appears for

$$\beta > \beta_{\mathrm{SchInt}} \equiv 0.28 \tag{4.12}$$

For the precursory collapse to happen in a realistic situation, these values of β must be physically feasible. There is a model-independent limit on the compactness of a neutron star, known as the Buchdahl theorem [5], given by

$$\beta < \beta_{\mathrm{Buch}} = \frac{4}{9} = 0.44 \tag{4.13}$$

Since $\beta_{\mathrm{SchInt}} < \beta_{\mathrm{Buch}}$, the precursory collapse can happen for physically realisable constant-density neutron stars.

Unlike single-horizon neutron star-black hole fusions, in precursory collapse mergers it is possible to define the pinch-on event (like in binary black holes) as the spacetime point at which the induced and supermassive black hole make contact. Furthermore, another event stands out: the creation of the induced black hole. Although the symmetries of the

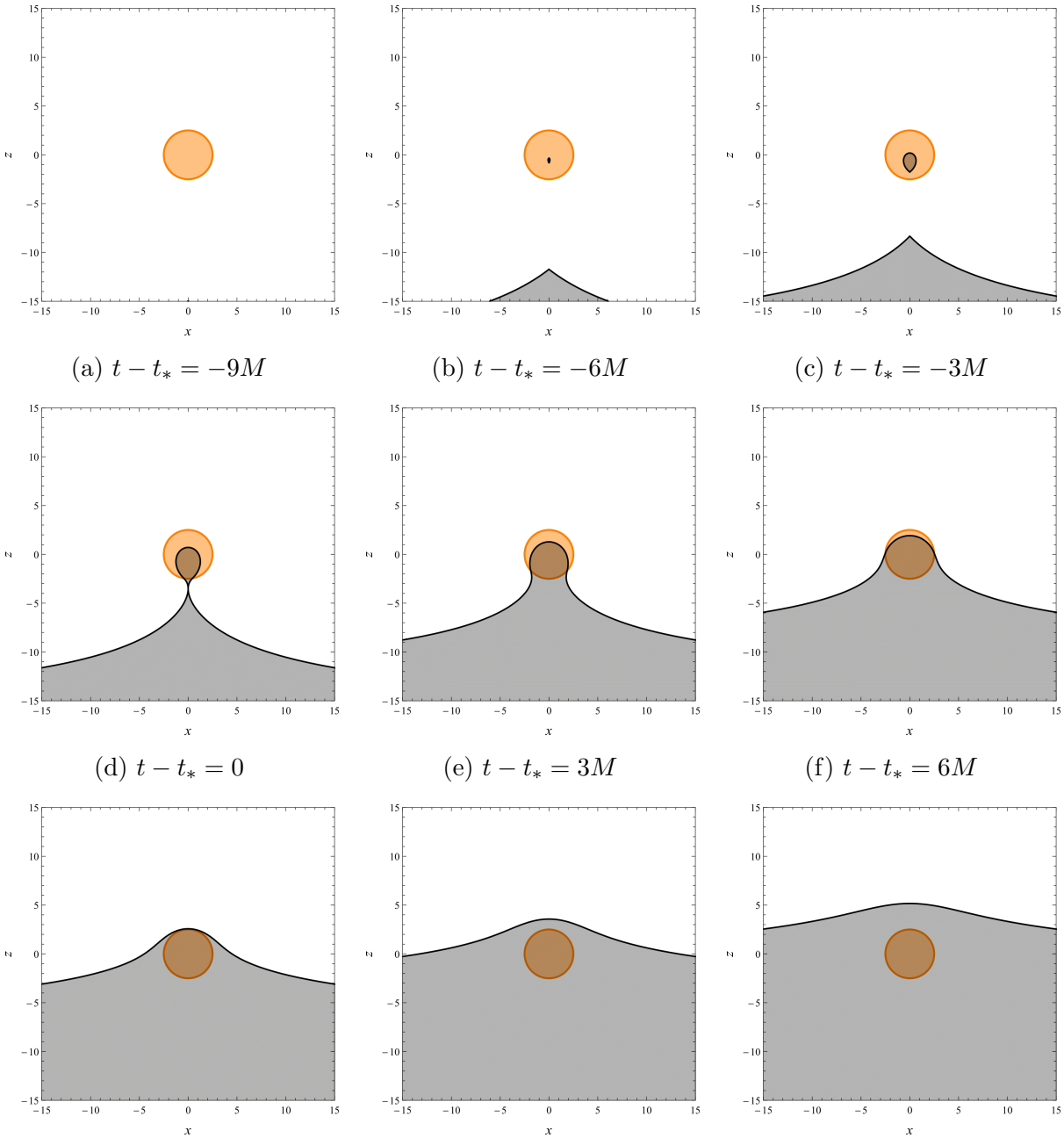

(a) $t - t_* = -9M$ (b) $t - t_* = -6M$ (c) $t - t_* = -3M$

(d) $t - t_* = 0$ (e) $t - t_* = 3M$ (f) $t - t_* = 6M$

(g) $t - t_* = 9M$ (h) $t - t_* = 12M$ (i) $t - t_* = 15M$

Figure 4.2: Constant-time slices of the event horizon in a merger of a supermassive black hole (down) with a constant-density neutron star (centre) of mass $M = 1$ and radius $R = 2.5$ ($\beta = 0.4$), in the latter's centre-of-mass reference frame. This merger presents a precursory collapse. The event horizon is plotted with a black line, the grey area represents the inside of the black holes and the star is drawn in orange. The axes are measured in units of M. The time slices are taken at regular time intervals.

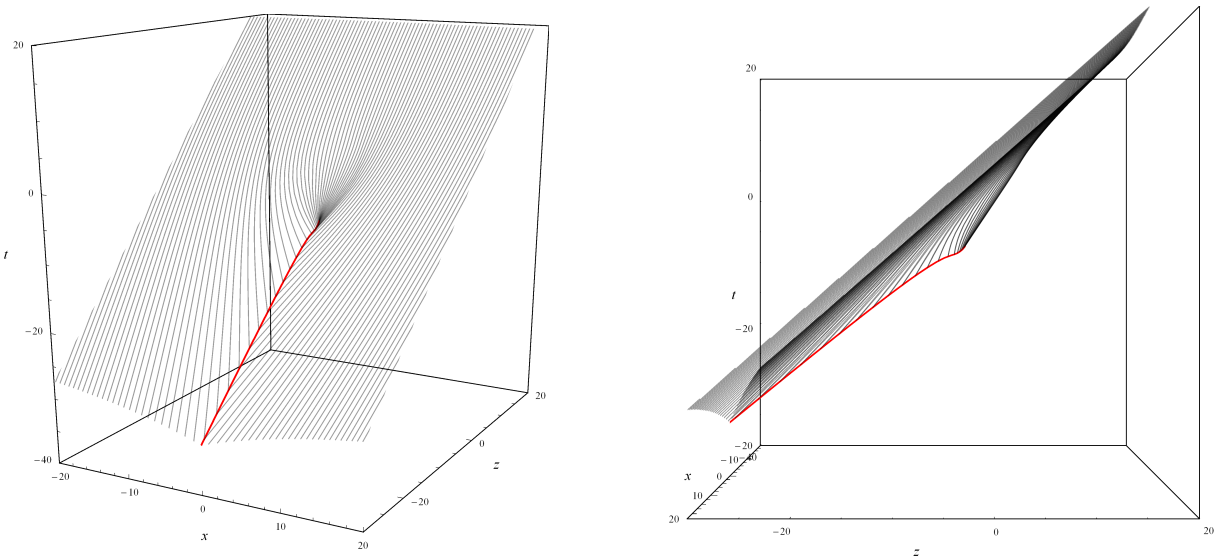

(a) (b)

Figure 4.3: Event horizon in a merger of a supermassive black hole with a constant-density neutron star of $R = 4$, $M = 1$ ($\beta = 0.25$). This merger does not present a precursory collapse. The red curve represents the caustic line. The axes are measured in units of M.

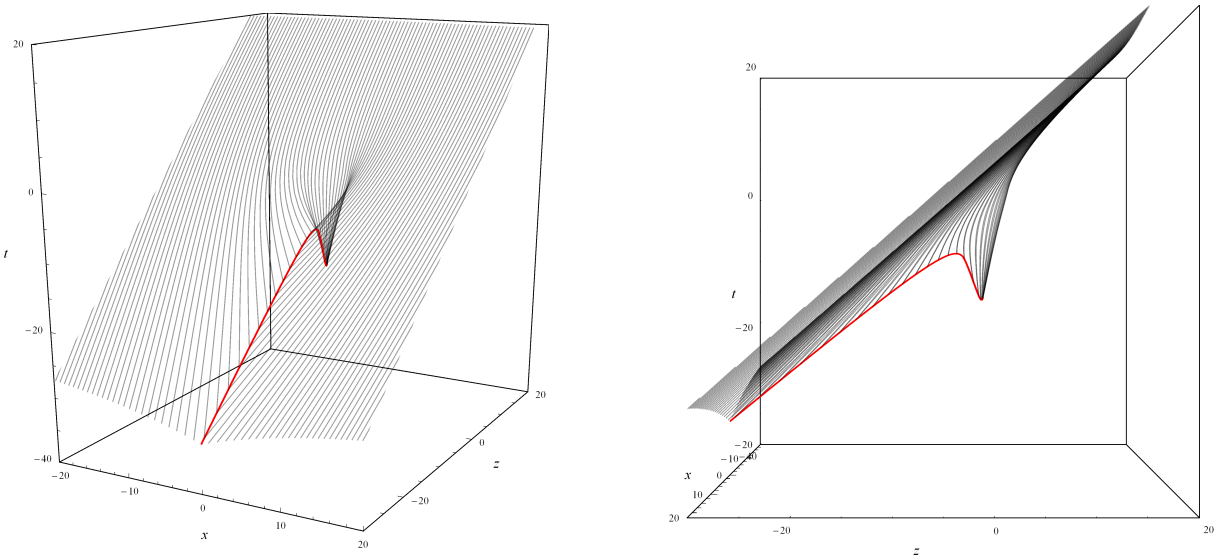

(a) (b)

Figure 4.4: Event horizon in a merger of a supermassive black hole with a constant-density neutron star of $R = 2.5$, $M = 1$ ($\beta = 0.4$). This merger presents a precursory collapse. The red curve represents the caustic line. The axes are measured in units of M.

merger guarantee that the time origin is arbitrary, the duration of the induced collapse can be invariantly characterised as the time interval between these events. For the case of figures 4.2, 4.4 ($\beta = 0.4$), we have

$$t_{\text{coll}} = 6.49475 \tag{4.14}$$

This duration depends on the compactness and diverges when it tends to the Buchdahl limit.

4.3 Tolman VII interior solution

The models developed above may have shown us the general properties of neutron stars and black hole mergers, but it is key to determine whether those hold for realistic situations. The way that we will do so will be to consider an accurate enough interior model. For our purposes, we have chosen the Tolman VII model [16]. This model presents the following advantages

- Although relatively complicated, it is analytical
- As in the above cases, the merger is fully characterised by a single parameter (β)
- A posteriori analyses [6, 13] prove that it is a valid model to describe realistic neutron stars, provided that the input parameters M, R have realistic values

The Tolman VII metric is

$$g_{tt} = -C_1 \cos^2\left[C_2 - \frac{1}{2}\log\left(\frac{r^2}{R^2} - \frac{5}{6} + \sqrt{\frac{R}{3Mg_{rr}}}\right)\right] \tag{4.15}$$

$$g_{rr} = \left(1 - \frac{Mr^2}{R^3}\left(5 - 3\frac{r^2}{R^2}\right)\right)^{-1} \tag{4.16}$$

with

$$C_1 = 1 - \frac{5M}{3R} \qquad ; \qquad C_2 = \arctan\sqrt{\frac{M}{3(R-2M)}} + \frac{1}{2}\log\left(\frac{1}{6} + \sqrt{\frac{R-2M}{3M}}\right) \tag{4.17}$$

and the metric continuity factor

$$\chi = \sqrt{\frac{1}{C_1}\left(1 - \frac{2M}{R}\right)}\cos^{-1}\left[C_2 - \frac{1}{2}\log\left(\frac{1}{6} + \sqrt{\frac{R-2M}{3M}}\right)\right] \tag{4.18}$$

As can be seen in figures 4.5, 4.6 and 4.7, the general structure of the merger is the same as for the other simpler models. In order to determine whether the precursory collapse is a real, physical process, let us characterise whether it happens for realistic values of the compactness. The bounds on β for a Tolman VII neutron star are more stringent than the Buchdahl limit, namely $\beta < 0.2698$ when we require the sound speed to be subluminal. Our computations yield that we have precursory collapse for any β

$$\beta > \beta_{\text{TVII}} \equiv 0.22 \tag{4.19}$$

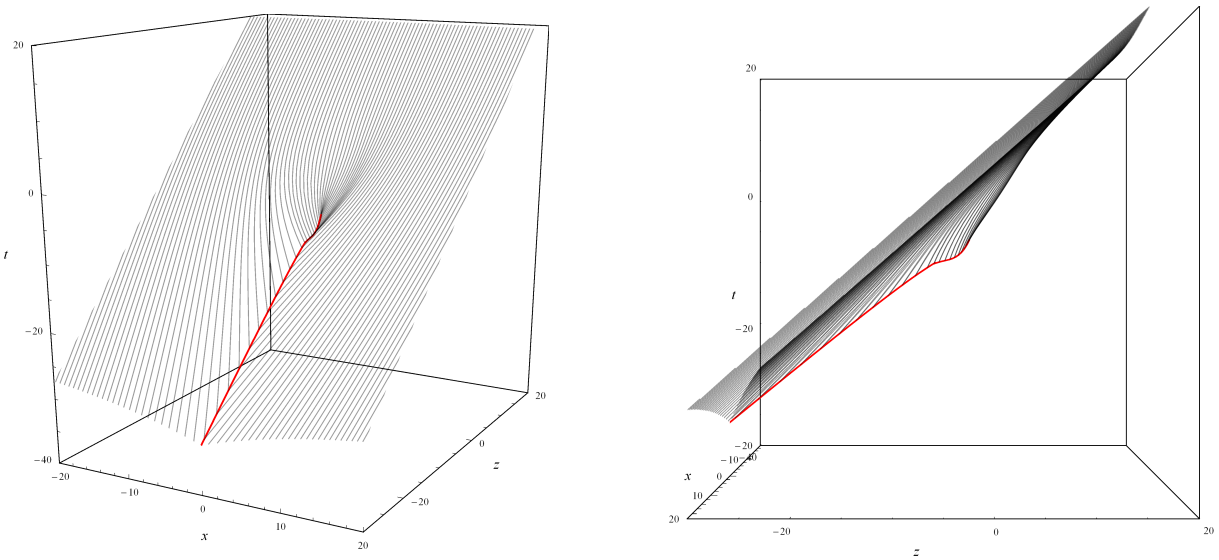

(a) (b)

Figure 4.5: Event horizon in a merger of a supermassive black hole with a realistic Tolman VII neutron star of $R = 5$, $M = 1$ ($\beta = 0.2$). This merger does not present a precursory collapse. The red curve represents the caustic line. The axes are measured in units of M.

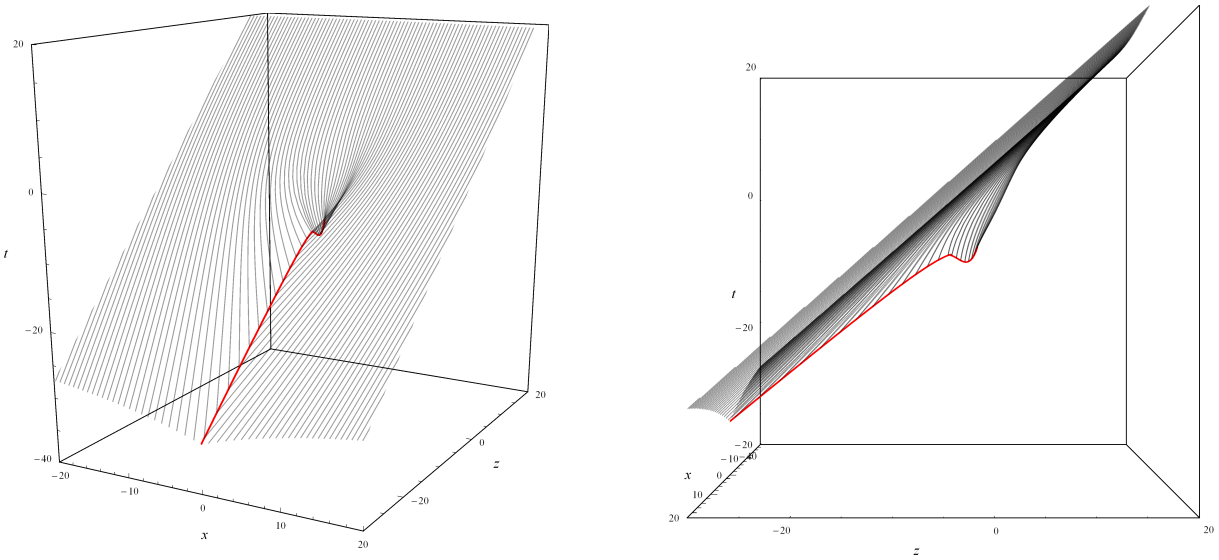

(a) (b)

Figure 4.6: Event horizon in a merger of a supermassive black hole with a realistic Tolman VII neutron star of $R = 4$, $M = 1$ ($\beta = 0.25$). This merger presents a precursory collapse. The red curve represents the caustic line. The axes are measured in units of M.

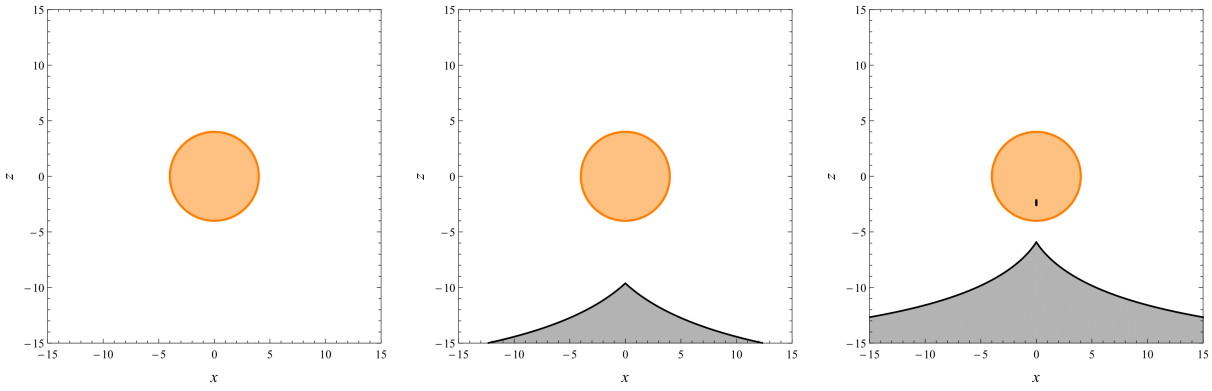

(a) $t - t_* = -9M$ (b) $t - t_* = -4M$ (c) $t - t_* = -1M$

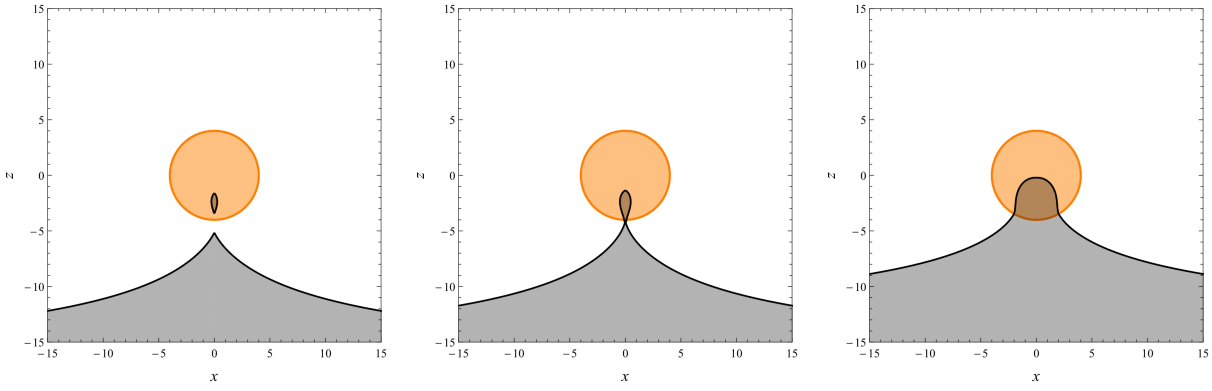

(d) $t - t_* = -0.5M$ (e) $t - t_* = 0$ (f) $t - t_* = 3M$

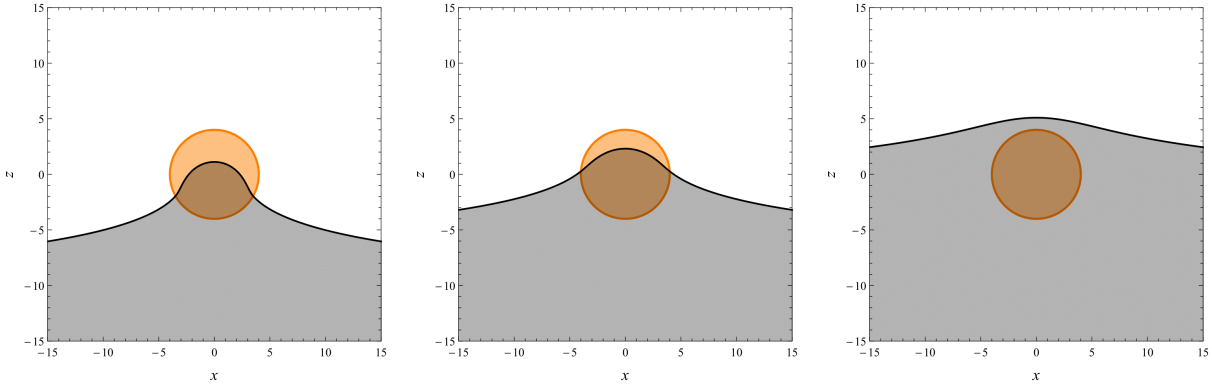

(g) $t - t_* = 6M$ (h) $t - t_* = 9M$ (i) $t - t_* = 15M$

Figure 4.7: Constant-time slices of the event horizon in a merger of a supermassive black hole (down) with a realistic Tolman VII neutron star (centre) of mass $M = 1$ and radius $R = 4$ ($\beta = 0.25$), in the latter's centre-of-mass reference frame. This merger presents a precursory collapse. The event horizon is plotted with a black line, the grey area represents the inside of the black holes and the star is drawn in orange. The axes are measured in units of M.

Since $\beta_{\text{TVII}} < 0.2698$, we have shown that the precursory collapse is a physical process that can happen in nature. The fact that the precursory collapse is a real process constitutes the most important point of this work and is the core idea in our paper [7], which we have submitted for publication.

As for the case of a constant-density neutron star, we can compute the duration of the precursory collapse. For the case of figures 4.6, 4.7 ($\beta = 0.25$), we have

$$t_{\text{coll}} = 2.05038 \tag{4.20}$$

This duration depends on the compactness and diverges when $\beta \to 0.2698$ (when the sound speed tends to 1).

4.4 Model-independent bound for precursory collapse

The above computations prove that the precursory collapse can happen in realistic situations, but the bounds on the compactness (4.12) and (4.19) are referred to interior models. It will be interesting, then, to obtain a model-independent bound on the compactness β_{s} such that for any $\beta > \beta_{\text{s}}$ there is precursory collapse.

Our argument for this bound is as follows: any neutron star and, in general, any spherical object that is not collapsing, must have its radius R larger than its Schwarzschild radius $R_{\text{Sch}} = 2M$. From the very broad assumptions used above (that the object is spherical, uncharged and static) we can assure that at $r > R$ the merger is equal to a merger with a Schwarzschild black hole. Therefore, if the maximum of the caustic line (pinch-on) in a merger of a supermassive black hole with a Schwarzschild black hole of mass M happens at a r_* such that $r_* > R$, then all possible models of neutron stars with M, R will have precursory collapse.

Note that the exact value of r_* has already been computed in (3.12) and is as follows

$$r_* = 3.52061M \tag{4.21}$$

Thus, any possible model of neutron stars will have precursory collapse at

$$\beta > \beta_{\text{s}} \equiv \frac{M}{r_*} = 0.28404 \tag{4.22}$$

This model-independent bound for precursory collapse has two key features: foremost, it does not depend on the mass (it is scale invariant). Secondly, it is smaller than the Buchdahl limit, so it constitutes yet another argument on the physical reality of precursory collapses.

5 Discussion

In this Master's thesis we have presented a general method for computing the event horizon in a compact binary coalescence in the extreme-mass-ratio. The original approach was developed in [8], but the novelty in this thesis is that we have extended the method to arbitrary infalling massive objects which are not necessarily black holes. This method is straightforward and computationally light, so it can be used to analyse the causal structure of a wide variety of mergers, including models for known objects or new exotic objects that have not yet been discovered.

To prove the usefulness of the method, we have used it to study the event horizon in mergers with a charged black hole and mergers with a neutron star. For the charged black holes, we have reproduced the analysis and recovered a similar structure than in the uncharged case whenever $|Q| \leq M$. For $|Q| > M$ (charged singularity), we see that the event horizon of the large black hole grows a "hole" itself, which we associate with a failure of the classical Einstein-Maxwell theory to take into account effects of quantum electrodynamics sufficiently close to the charge. For the neutron stars, we have discovered that the structure of the merger depends on the compactness of the star. Whenever this value is above a certain threshold, the merger develops a "precursory collapse", which means that the larger black hole induces the creation of a black hole in the star's interior and the merger happens "inside-out". This Master's thesis constitutes the first realisation of this effect and has therefore given rise to an article that we have submitted for publication. Furthermore, we derive certain observables for mergers with a neutron star, including model-specific and a model-independent bounds on the compactness to have a precursory collapse.

Further research is needed to fully characterise these compact binary coalescences. In particular, it would be of great interest to relax the extreme-mass-ratio assumption and work in a M/M_{SMBH} expansion. Many interesting effects that have been lost in our analysis could be recovered including, but not limited to, gravitational waves and tidal forces. Furthermore, a matched asymptotic expansion could be carried out between our EMR analysis at $M_{\text{SMBH}} \to \infty$ and the analysis at $M \to 0$ used to obtain gravitational wave templates.

Bibliography

[1] B. P. Abbott et al. Searches for gravitational waves from known pulsars with Science Run 5 LIGO data. *The Astrophysical Journal*, 713(1):671–685, mar 2010.

[2] B. P. Abbott et al. Observation of gravitational waves from a binary black hole merger. *Phys. Rev. Lett.*, 116:061102, Feb 2016.

[3] B.P. Abbott et al. GWTC-1: A gravitational-wave transient catalog of compact binary mergers observed by LIGO and Virgo during the first and second observing runs. *Phys. Rev. X*, 9(3):031040, 2019.

[4] J. Bally and E. R. Harrison. The electrically polarized universe. *The Astrophysical Journal*, 220:743, March 1978.

[5] H. A. Buchdahl. General relativistic fluid spheres. *Phys. Rev.*, 116:1027–1034, Nov 1959.

[6] M.S.R. Delgaty and Kayll Lake. Physical acceptability of isolated, static, spherically symmetric, perfect fluid solutions of einstein's equations. *Computer Physics Communications*, 115(2-3):395–415, Dec 1998.

[7] Roberto Emparan and Daniel Marin. Precursory collapse in neutron star-black hole mergers. 4 2020.

[8] Roberto Emparan and Marina Martinez. Exact event horizon of a black hole merger. *Class. Quant. Grav.*, 33(15):155003, 2016.

[9] Roberto Emparan, Marina Martínez, and Miguel Zilhão. Black hole fusion in the extreme mass ratio limit. *Physical Review D*, 97(4), Feb 2018.

[10] GraceDB - Gravitational-Wave Candidate Event Database. `https://gracedb.ligo.org`. Accessed: April 26, 2020.

[11] GW190412: Observation of a binary-black-hole coalescence with asymmetric masses. 4 2020.

[12] G. Nordström. On the energy of the gravitation field in Einstein's theory. *Koninklijke Nederlandse Akademie van Wetenschappen Proceedings Series B Physical Sciences*, 20:1238–1245, January 1918.

[13] Ambrish M. Raghoonundun and David W. Hobill. The geometrical structure of the Tolman VII solution. 2016.

[14] Hans Reissner. Über die eigengravitation des elektrischen feldes nach der einsteinschen theorie. *Annalen der Physik*, 355:106 – 120, 03 2006.

[15] Bernard F. Schutz. *A first course in General Relativity.* Cambridge Univ. Pr., Cambridge, UK, 1985.

[16] Richard C. Tolman. Static solutions of Einstein's field equations for spheres of fluid. *Phys. Rev.*, 55:364–373, Feb 1939.